The Ocean Circulation in Thermohaline Coordinates

JAN D. ZIKA, MATTHEW H. ENGLAND, AND WILLEM P. SIJP

Climate Change Research Centre, The University of New South Wales, Sydney, New South Wales, Australia

ABSTRACT

The thermohaline streamfunction is presented. The thermohaline streamfunction is the integral of transport in temperature–salinity space and represents the net pathway of oceanic water parcels in that space. The thermohaline streamfunction is proposed as a diagnostic to understand the global oceanic circulation and its role in the global movement of heat and freshwater. The coordinate system used filters out adiabatic fluctuations. Physical pathways and ventilation time scales are naturally diagnosed, as are the roles of the mean flow and turbulent fluctuations. Because potential density is a function of temperature and salinity, the framework is naturally isopycnal and is ideal for the diagnosis of water-mass transformations and advective diapycnal heat and freshwater transports. Crucially, the thermohaline streamfunction is computationally and practically trivial to implement as a diagnostic for ocean models. Here, the thermohaline streamfunction is computed using the output of an equilibrated intermediate complexity climate model. It describes a global cell, a warm tropical cell, and a bottom water cell. The streamfunction computed from eddy-induced advection is equivalent in magnitude to that from the total advection, demonstrating the leading-order importance of parameterized eddy fluxes in oceanic heat and freshwater transports. The global cell, being clockwise in thermohaline space, tends to advect both heat and salt toward denser (poleward) water masses in symmetry with the atmosphere's poleward transport of moisture. A reprojection of the global cell from thermohaline to geographical coordinates reveals a thermohaline circulation reminiscent of the schematized "global conveyor."

1. Introduction

It has long been recognized that the ocean displays variability across a large spectrum of spatial scales, from global-scale oceanic gyres and circumpolar currents to millimeter-scale turbulent motions, and on myriad temporal scales from millennial overturning to waves with microsecond periods (Davis et al. 1981). All temporal and spatial scales of motion contribute to the global ocean circulation and its role in the climate system (Munk and Wunsch 1998). Despite this, descriptive oceanographers have identified specific pathways of net oceanic motion from observed tracers fields (Wüst 1935; Deacon 1937; Gordon 1986). These pathways have been schematized in a variety of ways, with the "global conveyor" of Broecker (1991) being the most universally recognized (see Richardson 2008, for a review of such schematics).

Over the past half century, numerical models have moved to finer and finer resolution and have progressively resolved an increasing number of scales. A key challenge remains, however: distilling the plethora of motions of a numerical model into simplified indices and diagrams with minimal loss of information. It is also pertinent to test integral metrics of the ocean circulation and quantify how they relate to the climate system.

A common way of understanding the global circulation is to average oceanic velocities at constant latitude and depth and look at the circulation in a meridional–vertical coordinate. The circulation revealed is known as the meridional overturning circulation (MOC; Kuhlbrodt et al. 2007). The MOC describes net vertical and meridional motion. It is often used to infer how the ocean distributes properties around the globe by transposing the diagnosed MOC onto zonally averaged quantities. This approach is somewhat valid in the North Atlantic, where a strong mean overturning exists and properties are reasonably homogeneous at constant depth and latitude. In other regions, however, overturning cells in the depth–latitude plane do not correspond to property transports at all. In the Southern Ocean, for example,

Corresponding author address: Jan D. Zika, Climate Change Research Centre, The University of New South Wales, Sydney 2037, NSW, Australia.
E-mail: j.zika@unsw.edu.au

a vigorous "Deacon cell" exists, apparently driving 30–40 Sv (1 Sv $\equiv 10^6$ m^3 s^{-1}) of light surface water down to the depth of Drake Passage at around 2000 m (Manabe et al. 1990). However, when the circulation is averaged in density–latitude space, correlations between the meridional velocity and the thickness of density layers counter the Deacon cell (Döös and Webb 1994). Thus, by averaging the flow in density, rather than depth space, a complimentary view, more consistent with the distribution of tracers, is revealed.

In the example of the Southern Ocean, the vertical coordinate, density, is used to capture meridional exchanges of water masses. Nycander et al. (2007) and Nurser and Lee (2004) propose diagnosing the ocean circulation in density–depth coordinates to capture the vertical exchanges of water masses. Using this approach, J. D. Zika et al. (2011, unpublished manuscript) demonstrate that the processes that contribute to meridional exchanges of water masses in the Southern Ocean can be very different to those that contribute to vertical exchanges. Boccaletti et al. (2005) and Ferrari and Ferreira (2011) have analyzed the meridional circulation in temperature–latitude coordinates and reveal a different circulation to that in density–latitude coordinates.

Observed tracer distributions reveal oceanic exchanges of both heat and salt that are not only meridional but also zonal, between ocean basins, and vertical, between the ocean surface and the interior (e.g., Broecker 1991; Gordon 1991; Schmitz 1996). We seek a coordinate system that captures this net global circulation.

Principally, the ocean circulation is considered important in the climate system because of its role in transporting heat, freshwater, nutrients, and carbon. By transporting heat and freshwater around the globe, the ocean influences global temperatures and plays a key role in the hydrological cycle. The water masses through which the global conveyor is thought to travel are each defined by unique temperature and salinity properties. Here, we investigate the ocean circulation in temperature–salinity (thermohaline) coordinates. By doing so, we are able to determine whether a global conveyor of the scale previously proposed based on observed tracer fields (Gordon 1986; Broecker 1991) exists in a climate model. In addition, we argue that such analysis provides a useful framework for the quantification of the thermohaline circulation, transit time scales, heat and moisture transport, geographical pathways, and the influence of parameterized and resolved turbulent motions.

This is not the first study to consider some aspect of ocean circulation in thermohaline coordinates. Speer (1993) relates air–sea heat and salt fluxes to a transformation rate (effectively advection) in thermohaline coordinates. Zika and McDougall (2008) and Zika et al. (2009) use a conservative temperature–neutral density coordinate (locally equivalent to a rotated conservative temperature–salinity coordinate) to understand the balance of advection and mixing in the ocean interior and have extended this to a general inverse method (Zika et al. 2010a,b). Some previous studies have analyzed numerical model output in a thermohaline coordinate (Cuny et al. 2002; Marsh et al. 2005). Indeed, Blanke et al. (2006) compute a streamfunction in thermohaline space for a regional model of the North Atlantic using Lagrangian particle tracking. An independent study by Döös et al. (2012) analyzes the circulation of a global ocean model following a similar methodology to that presented here. Although a different class of ocean model is used, including a resolution permitting eddies, Döös et al. (2012) find similar thermohaline cells to those described here.

Section 2 of this article defines the thermohaline streamfunction (THS) and describes how it can be easily diagnosed from a finite-volume ocean model. Section 3 describes the THS as diagnosed from a climate model. Section 4 discusses the Eulerian mean and fluctuating contributions to the THS, and in section 5 the calculation of advective diapycnal heat and salt fluxes is discussed. Section 6 describes the diagnosis of a thermohaline transit time, whereas section 7 shows a diagnosis of the THS for different basins and the use of the THS to infer water-mass pathways. We summarize the main conclusions in section 8.

2. The thermohaline streamfunction

Here, we review some standard streamfunction diagnostics used in the literature and then describe the computation of a thermohaline streamfunction.

a. Barotropic and meridional overturning streamfunctions

Take a flow in the three coordinates: longitude x, latitude y, and height z, bounded by (x_1, x_2), (y_1, y_2), and $[-H(x, y), \eta(x, y)]$, respectively, with velocity $\mathbf{u} = (u, v, w)$. If we have

$$\nabla \cdot \mathbf{u} = 0, \tag{1}$$

we can define a streamfunction ψ_{xy} such that

$$\frac{\partial \psi_{xy}}{\partial y} = -\int_{-H}^{\eta} u \, dz; \quad \frac{\partial \psi_{xy}}{\partial x} = \int_{-H}^{\eta} v \, dz. \tag{2}$$

So long as $v = 0$ at $y = y_1$ (in the case of the global ocean, y_1 would be a latitude circle wholly inside the
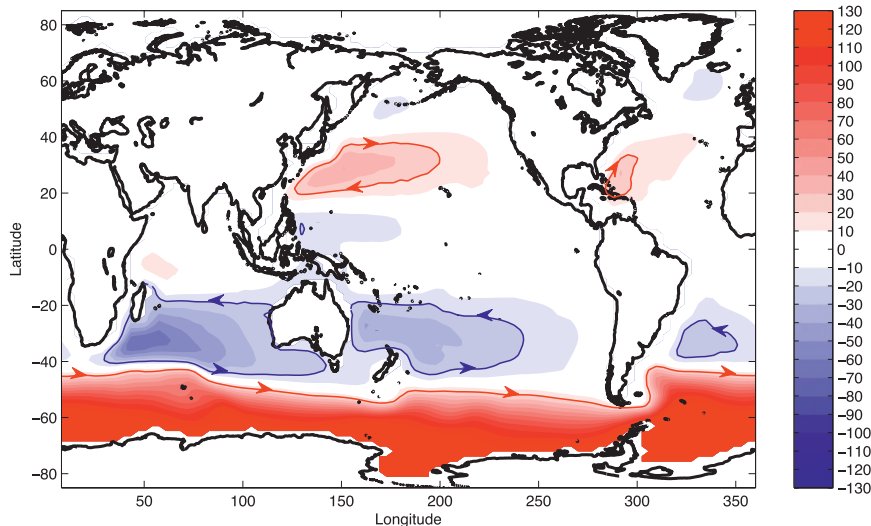
FIG. 1. Mean barotropic streamfunction Ψ_{xy} (Sv) from the ocean component of the final 10-yr average of a 3000-yr run of a climate model (described in section 3). The 20-(blue) and -20-Sv (red) contours are shown. The Ψ_{xy} is computed by integrating northward from the Antarctic, and the value at the African continent is then subtracted.

Antarctic continent), the streamfunction is diagnosed using

$$\psi_{xy}(x,y) = -\int_{y_1}^{y} \int_{-H}^{\eta} u(x, y', z)\, dz\, dy'. \qquad (3)$$

Here, ψ_{xy} is commonly known as the barotropic streamfunction. The barotropic streamfunction for an intermediate complexity climate model (to be discussed in detail in section 3) is plotted in Fig. 1. The barotropic streamfunction reveals the wind-driven basin-scale gyres, their boundary currents, and the pathway and strength of the Antarctic Circumpolar Current.

Alternatively, integrating at constant depth and latitude, one can derive a meridional overturning streamfunction ψ_{zy} such that

$$\frac{\partial \psi_{zy}}{\partial y} = -\int_{x_1}^{x_2} w\, dx; \qquad \frac{\partial \psi_{zy}}{\partial z} = \int_{x_1}^{x_2} v\, dx, \qquad (4)$$

and again, so long as $w = 0$ at $z = -H$ (e.g., below the deepest topography), ψ_{zy} can be diagnosed as

$$\psi_{zy}(y,z) = -\int_{-H}^{z} \int_{x_1}^{x_2} v(x, y, z')\, dx\, dz'. \qquad (5)$$

The meridional overturning streamfunction for an intermediate complexity climate model is plotted in Fig. 2. The meridonal overturning streamfunction reveals meridional cells of the MOC, linking the equatorial and poleward waters and the surface and deep waters. As

discussed in section 1, the MOC does not accurately represent the meridional exchanges of waters of different densities and temperatures. To diagnose such exchanges and infer the processes that contribute to those exchanges, it is illuminating to compute a streamfunction as a function of latitude and a second, time-evolving tracer. Following Ferrari and Ferreira (2011), we define a meridional streamfunction ψ_{Cy}, for an arbitrary tracer C, such that

$$\psi_{Cy} = \iint_{C' \le C} v\, dx\, dz, \qquad (6)$$

where $\int \int_{C' \le C} dx\, dz$ is the area over a surface of constant latitude, where $C' \le C$. The streamfunction ψ_{Cy} can be used to diagnose the advective meridional transport of C and to understand which mechanisms give rise to that transport (Ferrari and Ferreira 2011).

Equation (6) applied to an instantaneous velocity field gives an instantaneous streamfunction. In this case, the streamfunction represents not only the rate at which water parcels move from one concentration C to another but also the rate at which isosurfaces of constant C move in space. Averaging over some period Δt, we may diagnose a mean streamfunction Ψ_{Cy} such that

$$\Psi_{Cy} = \frac{1}{\Delta t} \int_{t}^{t+\Delta t} \iint_{C' \le C} v\, dx\, dz\, dt. \qquad (7)$$

Here and throughout, time-mean streamfunctions will be defined using a capital Ψ. Eulerian mean and fluctuating components will later be distinguished using $\overline{\Psi}$ and Ψ^*,
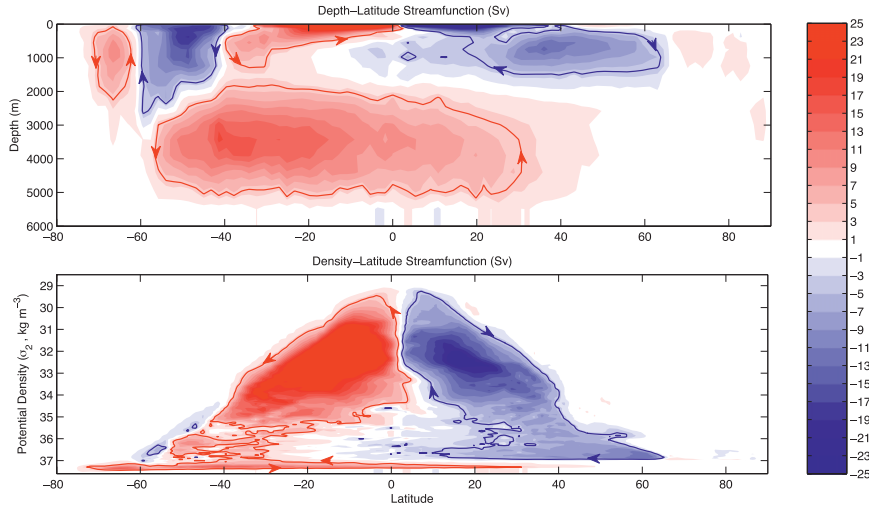
FIG. 2. (top) Mean depth–latitude streamfunction Ψ_{zy} (Sv) from the ocean component of a climate model (described in section 3). (bottom) Density–latitude streamfunction $\Psi_{\sigma_2 y}$ (Sv). The 4- (red) and −4-Sv (blue) streamlines are shown with solid contours.

respectively. As Ferrari and Ferreira (2011) point out, if C is steady over the period Δt [i.e., $\int_t^{t+\Delta t} (dC/dt) \, dt = 0$], then Ψ_{Cy} represents the flow of water from one C value to another. Whether the flow is steady, Ψ_{Cy} can still be diagnosed, and in the unsteady case it represents both the transformation of water parcels and the movement of the tracer (Nurser and Marsh 1998).

Here we compute the $\Psi_{y\sigma_2}$: that is, a streamfunction in potential density–latitude coordinates (we choose potential density referenced to 2000-m depth σ_2; Fig. 2b). The density–latitude streamfunction gives a complementary view of the circulation to the depth–latitude streamfunction (Fig. 2a). In particular the Deacon cell is reduced to 3–4 Sv in the density–latitude case. The parameterized eddy-induced velocity and zonal asymmetries allow a circulation to exist in the Southern Ocean in latitude–depth space without large exchanges of mass (density) across latitude circles. In addition, the bottom water cell around Antarctica and the deep "abyssal cell" below 2000-m depth are here linked together in one bottom water cell at σ_2 values greater than 37 kg m^{-3}.

What is not clear from the depth–latitude or the density latitude streamfunction is the geographical route taken by dense waters after they have sunk in formation regions such as the North Atlantic. Both diagnostics show a sinking around 60°N. Where these waters eventually upwell and which geographical regions they transit through (either isopycnally or diapycnally) is unclear.

b. A streamfunction in two general coordinates

We seek a streamfunction that is not solely meridional but can also encapsulate vertical and zonal motions as

well. As such, we compute a streamfunction $\psi_{C_1 C_2}$ in terms of two tracers, C_1 and C_2. Hence,

$$\psi_{C_1 C_2} = \int_{C_1' \leq C_1 |_{C_2}} (\mathbf{u} \cdot \mathbf{n}_{C_2}) \, dA, \qquad (8)$$

where $\mathbf{n}_{C_2}$ is the direction normal to a C_2 isosurface and $\int_{C_1' \leq C_1 |_{C_2}} dA$ is the area over the C_2 isosurface where $C_1' \leq C_1$. Again, the instantaneous $\psi_{C_1 C_2}$ represents both the transformation of water parcels from different tracer concentrations and the adiabatic movement of tracer isosurfaces (see Griffies 2007, 138–141, for a discussion of diasurface flow). The mean streamfunction in the C_1–C_2 coordinate is then

$$\Psi_{C_1 C_2} = \frac{1}{\Delta t} \int_t^{t+\Delta t} \int_{C_1' \leq C_1 |_{C_2}} (\mathbf{u} \cdot \mathbf{n}_{C_2}) \, dA \, dt. \qquad (9)$$

In this study, we will only consider cases where tracers are statistically steady. Interpretations of unsteady streamfunctions are left to future work.

Note that a streamfunction $\Psi_{C_1 C_2}$ can be formulated for isosurfaces of constant C_1 where $\Psi_{C_1 C_2} = -\Psi_{C_2 C_1}$. Replacing C_2 with the meridional coordinate y, (9) is equivalent to (7) as $\mathbf{u} \cdot \mathbf{n}_y = v$. Indeed, one could also replace C_1 with the vertical coordinate z and recover the mean of the latitude–depth overturning Ψ_{yz} [(5); i.e., the meridional overturning streamfunction]. Hence, (9) represents a general equation for a streamfunction in two coordinates, whether in standard geographical coordinates or coordinates defined by time-variable tracers.

For the remainder of this study, we will consider oceanic flow in thermohaline coordinates: that is, where
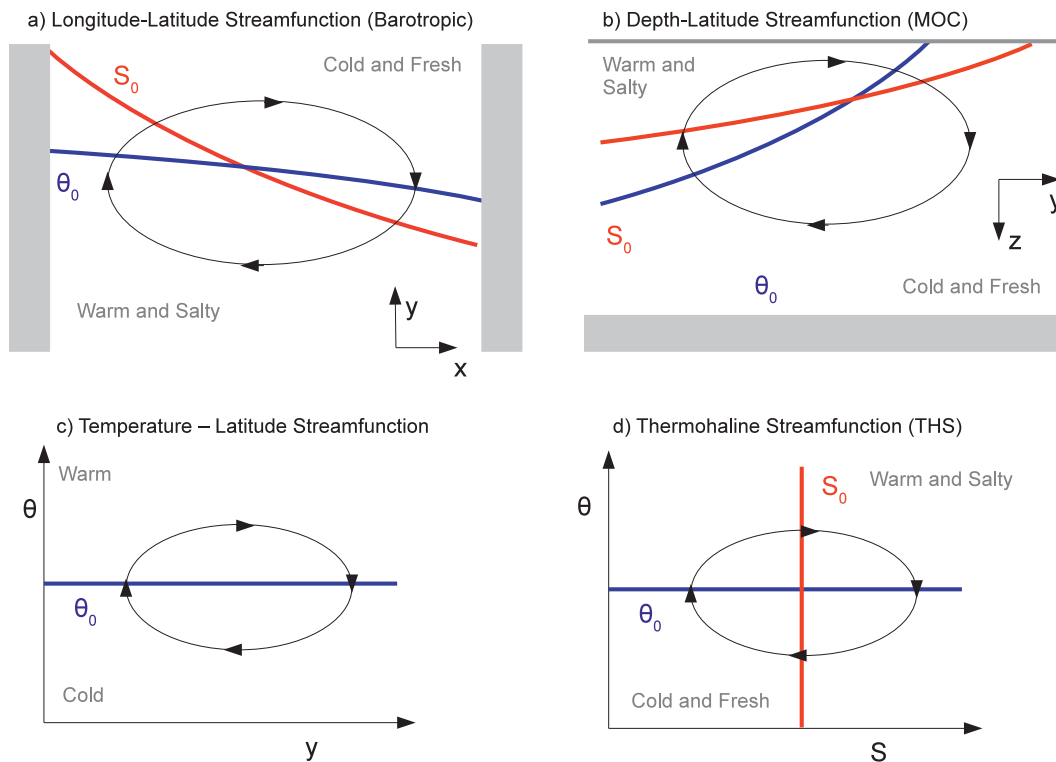
FIG. 3. Schematic describing four streamfunction diagnostics: (a) barotropic streamfunction showing horizontal motion, (b) meridional overturning streamfunction showing vertical motion, (c) temperature–latitude streamfunction showing net effect of horizontal motion in transporting heat meridionally, and (d) THS showing net effect of all motion in transporting water from regions of different temperatures and salinities. Overlaid in (a),(b),(d) are schematic isolines of constant potential temperature and salinity [at the surface in (a) and zonally averaged in (b)].

our two tracer variables are potential temperature θ and salinity S. The mean thermohaline streamfunction is given by

$$\Psi_{\theta S} = \frac{1}{\Delta t} \int_{t}^{t+\Delta t} \int_{\theta' \le \theta|_S} (\mathbf{u} \cdot \mathbf{n}_S) \, dA \, dt. \qquad (10)$$

In practice, (9) could be applied to any three-dimensional (3D), incompressible flow. We use θ and S because these are the variables that describe heat and salt content, respectively, in our model. In calculations based on more precise models or observations, the appropriate heat variable is conservative temperature Θ (McDougall 2003) and the appropriate salt variable is absolute salinity S_A (McDougall et al. 2009).

If the flow and tracer distributions are steady, $\Psi_{\theta S}(S, \theta)$ represents the transformation of water masses from different temperature and salinity values: that is, the warming and freshening of water parcels as they move through the ocean. This conversion need not be diapycnal because water parcels can have compensating changes in heat and salt and remain at the same density.

Schematically represented in Fig. 3 are four streamfunctions: two in fixed geographical coordinates, x–y and z–y; one with a time-variable vertical coordinate, θ–y; and finally the θ–S streamfunction in purely time-variable coordinates. The flow in Fig. 3 is reminiscent of both a midlaltitude gyre and diffusively upwelled thermohaline conveyor (Stommel and Arons 1960). A gyre circulation moves warm salty waters poleward (Fig. 3a). The warm salty water then cools, becoming cold and salty. The surface waters then freshen with some sinking into the deep ocean (Fig. 3b). The surface gyre circulation warms and evaporates as it moves southward, becoming warm and salty again (Fig. 3a). The deep portion warms and freshens via interior mixing as it upwells (Fig. 3b). Averaging at constant latitude, we see that this circulation transports warm water northward and cold water southward (Fig. 3c). Averaging in temperature–salinity space, we see that both the gyre circulation and the diffusively upwelled overturning involve a circulation from warm and fresh to warm and salty, then cold and salty, then cold and fresh, and back to warm and fresh.

c. Computing the thermohaline streamfunction of an ocean model

Ocean models do not describe a continuous flow field and temperature and salinity distributions but rather a discretized approximation of it. The most common discretization is one where the equations of motion and property conservation are solved on a grid defined by finite volumes. For each volume, a property concentration is assigned, as are transports across grid volume interfaces.

Here, we describe how $\Psi_{\theta S}$ is calculated from a finite-volume ocean model. Consider a model with $1{:}N$ grid-box interfaces and $1{:}M$ discrete time steps. For a given model, we require the volume fluxes U_{ij} across all grid-box interfaces i at time steps j. These are determined from the velocity at the interface and the interface area [e.g., $U = (u\Delta y\Delta z;\ v\Delta x\Delta z;\ w\Delta x\Delta y)$ for longitudinal, latitudinal, and vertical grid spacings Δx, Δy, and Δz, respectively]. To determine the streamfunction in thermohaline coordinates, we also require temperatures at the grid interfaces θ_{ij} and the salinities of the adjoining grid boxes S_{ij}^{+} and S_{ij}^{-}. The volume fluxes and temperatures at the interfaces, and salinities of the adjoining grid boxes are stored in computer memory. Then, over all time steps the thermohaline streamfunction is computed using

$$\Psi_{\theta S}(S,\theta) = \frac{1}{M}\sum_{i=1}^{M}\sum_{j=1}^{N}\delta_{ij}^{\theta}\delta_{ij}^{S}U_{ij},$$

$$\delta_{ij}^{\theta} = \begin{cases} 1 & \text{if}\quad \theta_{ij} <= \theta, \\ 0 & \text{otherwise.} \end{cases}$$

$$\delta_{ij}^{S} = \begin{cases} 1 & \text{if}\quad S_{ij}^{+} > S \quad\text{and}\quad S_{ij}^{-} < S, \\ -1 & \text{if}\quad S_{ij}^{+} < S \quad\text{and}\quad S_{ij}^{-} > S, \\ 0 & \text{otherwise.} \end{cases}$$

(11)

Above, the delta function δ^{θ} eliminates from the calculation all interfaces where $\theta_i > \theta$ and δ^{S} eliminates fluxes that do not cross the S isosurface. It also sets the sign of the flux, depending on whether the flow is up gradient or down gradient.

Figure 4 shows how a thermohaline streamfunction $\Psi_{\theta S}$ is calculated from a discretized field. In Fig. 4, the grid boxes where $\delta^{S}\delta^{\theta} = 1$ or -1 are those along the light blue line in Fig. 4c between $S' < S$ and $S' > S$ with $\theta' < \theta$. Computing $\Psi_{\theta S}$ for a velocity field such as the output of an ocean model, we effectively integrate over all water masses with like properties in time and space.

3. The thermohaline streamfunction of a climate model

We diagnose the ocean component of the final 10 yr of a 3000-yr simulation of the University of Victoria Climate Model (1.8° latitude by 3.6° longitude grid spacing,

19 levels, and 2D energy balance atmosphere) as used by (Sijp et al. 2006: specifically their case referred to as "GM"). The ocean model is the Geophysical Fluid Dynamics Laboratory (GFDL) Modular Ocean Model version 2.2 (MOM2; Pacanowski 1995). The vertical mixing coefficient increases with depth, taking a value of 0.6×10^{-4} m^2 s^{-1} at the surface and increasing to 1.6×10^{-4} m^2 s^{-1} at the bottom. The model employs the eddy-induced advection parameterization of Gent and McWilliams (1990) with a constant diffusion coefficient of 1000 m^2 s^{-1}. The advective velocity due to this parameterization will be referred to with the superscript GM. Tracers are diffused in the isopycnal direction with a constant coefficient of 2000 m^2 s^{-1}.

The ocean model displays a plausible global θ–S distribution and MOC and by the year 3000 the ocean model has reached a stable equilibrium. This model is typical of those used to understand different climate states and the stability of the global overturning circulation. As in all such ocean climate models, the model MOC displays several isolated cells including a shallow clockwise (north) and an anticlockwise (south) cell in the tropics, a Northern Hemisphere deep cell, a bottom water cell toward Antarctica, a Deacon cell between 60° and 40°S, and finally an abyssal cell below 2000-m depth.

A scatterplot of ocean θ–S with a color code corresponding to ocean basin and latitude allows one to relate points in θ–S space to particular geographical regions (Fig. 5). The warmest and saltiest waters are found in the North Atlantic (red), as are colder salty waters reaching below 5°C (red). The coldest and freshest waters are found in the Arctic (red), cold and modestly fresh waters are found in the Southern Ocean (yellow), and fresh but generally slightly warmer waters are found in the North Pacific (dark blue). The warmest waters are found in the equatorial Indo-Pacific (cyan). Only along a locus of water-mass classes, narrow in the saline coordinate, do waters from the three major ocean basins exist together.

In MOM2, velocities and tracer values are defined on a "B grid" such that the u and v velocity components are defined on the corners of each grid box. These velocities are linearly interpolated onto the gridbox interfaces (as is done in the advection scheme of the model). Tracer concentrations are defined at the center of each grid box. Hence, the temperatures at the gridbox interfaces are defined by linearly interpolating between grid boxes.

Using monthly velocity, potential temperature, and salinity fields, we compute the mean thermohaline streamfunction (Fig. 6). It reveals, as its dominant feature, a 15-Sv cell. This "global cell" reaches from the warm salty waters found only in the Atlantic through to the cold and fresh waters found largely in the Southern Ocean and then to the warm fresh waters found only in the Indo-Pacific
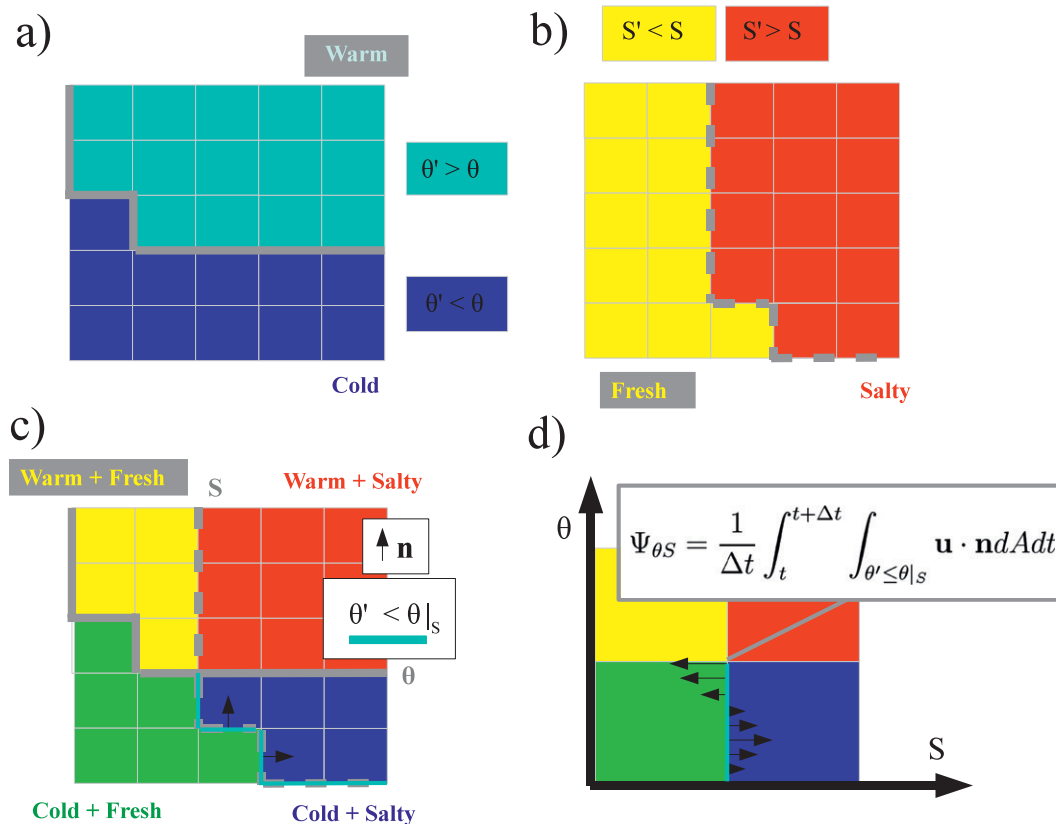
FIG. 4. Schematic describing the way the THS is computed from the output of a finite-volume ocean model. Model grid boxes are defined on some native coordinate (e.g., x and y or y and z) by their (a) potential temperature and (b) salinity. (c) Where potential temperature $\theta' < \theta$, all fluxes are summed across gridbox interfaces where flow is from salinity $S' < S$ to $S' > S$ in the native coordinate. (d) Summing these fluxes, a THS at (θ, S) is determined and represented in thermohaline coordinates.

basin. Two other counterclockwise cells appear in the THS. These are the very warm tropical cell ($\theta > 25°$C) with a transport of around 8 Sv and the very cold ($\theta < 2°$C) bottom water cell, also with a transport of around 8 Sv. Within the global cell lies a warm and a cold subcell, separated around the 10°C isotherm, each with an additional transport of 5–10 Sv.

North Atlantic Deep Water (NADW) is characterized in this model as having a potential temperature colder than 5°C and a salinity of around 35 g kg^{-1}. Only 4–6 Sv achieves such temperatures and salinities. NADW, at its coldest, is close to 2°C with a salinity of around 34.7 g kg^{-1}. Once formed, the NADW warms, presumably through entrainment and interior mixing. The NADW branch then joins the remaining streamlines heading toward colder fresher regions of the ocean. In section 6, we decompose this circulation by ocean basin.

A circulation of around 6 Sv links water masses found uniquely in the Atlantic, Southern Ocean, and Indo-Pacific (cf. Figs. 5, 6). The many vertical and horizontal circulations, once integrated in θ–S space, give rise to

one interconnected flow. In effect, this is a quantification of the global conveyor proposed by Broecker (1991).

4. Eddy-induced and seasonal transports

In the ocean model discussed here, as in virtually all contemporary ocean models that do not explicitly resolve eddy fluxes, tracers are advected by both an Eulerian mean velocity $\mathbf{u}^{EM}$ and an eddy-induced velocity $\mathbf{u}^{GM}$ such that

$$\mathbf{u} = \mathbf{u}^{EM} + \mathbf{u}^{GM}. \qquad (12)$$

The eddy-induced velocity is prescribed using the scheme of Gent and McWilliams (1990). In the MOC, $\mathbf{u}^{GM}$ is significant mainly in the Southern Ocean and North Atlantic where isopycnal slopes are very large. When computing the THS of Fig. 6, we used both the eddy-induced and Eulerian velocities and averaged these for each monthly field. We can now assess the influence of the Eulerian flow and the eddy-induced flow and the fluctuations actually resolved by the model by making the following decomposition:
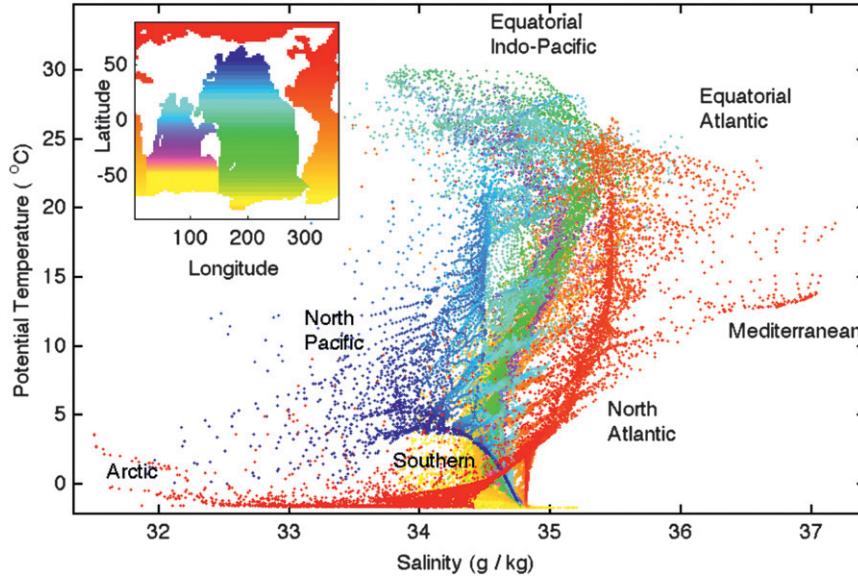
FIG. 5. Scatterplot of potential temperature and salinity from the mean state of the ocean model. Each grid box is represented by one dot in θ–S space. The color of each dot corresponds to its latitude and basin using the color code shown in the insert.

$$\overline{\Psi}_{\theta S}^{EM}(S, \theta) = \int_{\overline{\theta}' \leq \overline{\theta}|_{\overline{S}}} (\overline{\mathbf{u}^{EM}} \cdot \mathbf{n}) \, dA \, dt,$$

$$\overline{\Psi}_{\theta S}^{GM}(S, \theta) = \int_{\overline{\theta}' \leq \overline{\theta}|_{\overline{S}}} (\overline{\mathbf{u}^{GM}} \cdot \mathbf{n}) \, dA \, dt \qquad (13)$$

where the overline represents an Eulerian average (i.e., $\overline{\xi} = (1/\Delta t) \int_t^{t+\Delta t} \xi \, dt$ for some variable ξ).

At its peak, the Eulerian mean contribution to the thermohaline streamfunction, $\overline{\Psi}_{\theta S}^{EM}$, is 39 Sv (Fig. 7b). The global cell of the Eulerian plus eddy-induced THS is
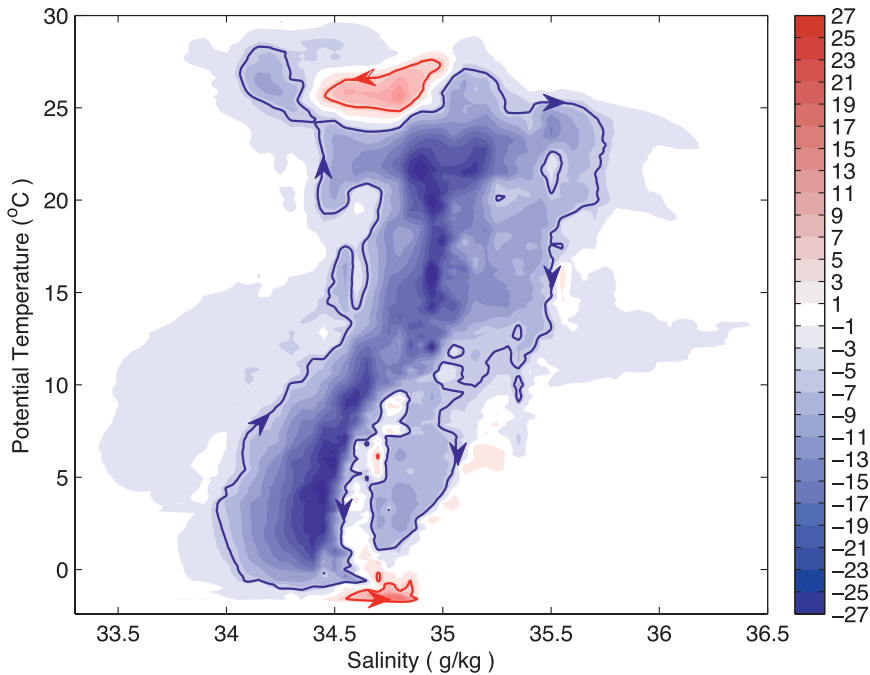
FIG. 6. THS $\Psi_{\theta S}$, derived from 10 yr of monthly, u, v, w, θ, and S fields of the ocean model. Positive values are anticlockwise and negative values are clockwise. The 4-Sv streamline is shown in red and the -4-Sv streamline is shown in in blue.
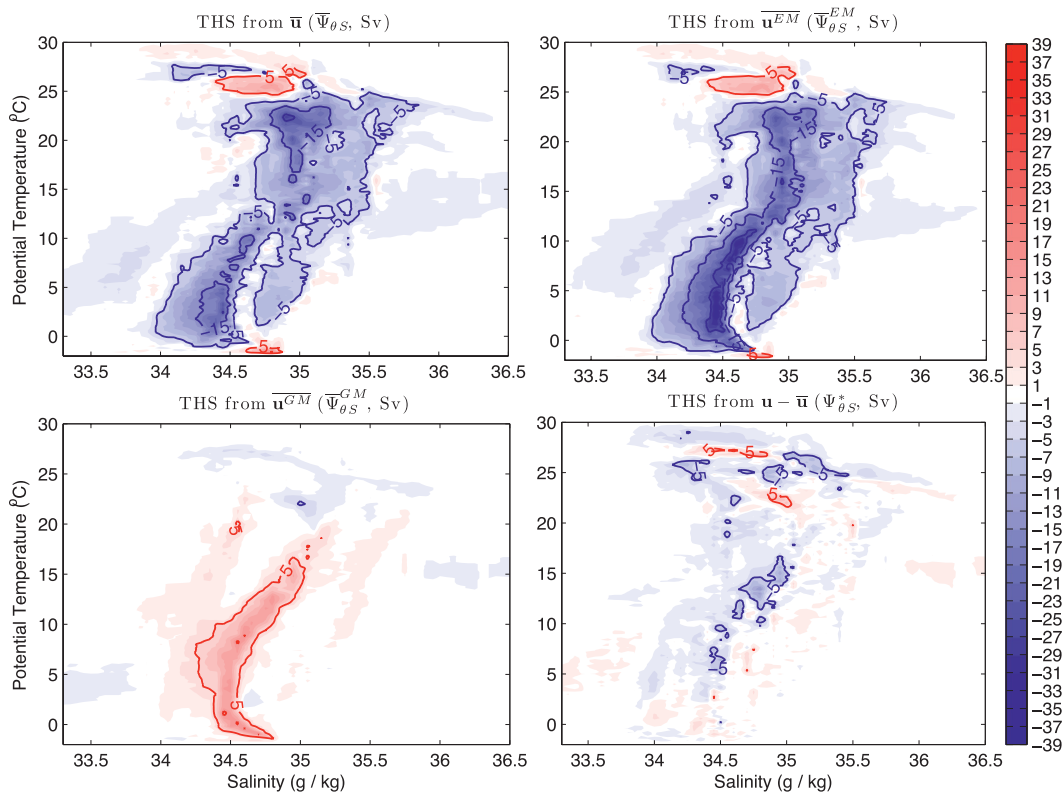
FIG. 7. (top left) THS from the sum of the time-mean Eulerian velocity and the time-mean eddy-induced velocity ($\overline{\mathbf{u}^{EM}} + \overline{\mathbf{u}^{GM}}$). (top right) THS from the time-mean Eulerian velocity. (bottom left) THS from the time-mean eddy-induced velocity. (bottom right) Difference between total THS and THS from the sum of the time-mean Eulerian and eddy-induced velocities: that is, the contribution to the THS due to resolved fluctuations such as the seasonal cycle.

15 Sv and peaks at 25 Sv in its subcells (Fig. 6). The Eulerian mean THS is compensated by an anticlockwise circulation due to the eddy-induced velocity of around 5–10 Sv (Fig. 7b). This compensation occurs across a significant fraction of the water-mass classes covered by the global THS cell ($-1°C > \theta > 15°C$ and $34 \text{ g kg}^{-1} > S > 35 \text{ g kg}^{-1}$). We find that, while $\mathbf{u}^{GM}$ is small across most latitudes, it is large where water flows from one water mass to another, particularly in the cooler fresher water masses associated with the Southern Ocean.

As above, the eddy-induced velocity is introduced to account for the effect of transient eddies not resolved on the 1.8° by 3.6° grid. The model does, however, resolve fluctuations on seasonal and interannual time scales, and hence we do expect a difference between $\Psi_{\theta S}$ and $\overline{\Psi}_{\theta S} = \overline{\Psi}_{\theta S}^{EM} + \overline{\Psi}_{\theta S}^{GM}$, with the difference being the role played by resolved temporal fluctuations ($\Psi_{\theta S}^*$; Fig. 7d). The major difference between the two is in the tropical waters ($\theta > 20°C$) and in the region linking the warm salty portion and the cold fresh portion of the global cell ($\theta \approx 15°C$ and $S \approx 35 \text{ g kg}^{-1}$). The ocean model used here is known to display a robust seasonal cycle but small interannual fluctuations. It is thus likely that, in this model

and perhaps in the real ocean, seasonal fluctuations contribute around 5 Sv of exchange between warm salty and cold fresh waters.

5. Diapycnal fluxes and thermohaline symmetry

By way of introduction to the idea of diagnosing the advective heat transport from a streamfunction, we again revisit Ferrari and Ferreira (2011), where their latitude–θ streamfunction $\Psi_{y\theta}$ can be used to diagnose the advective meridional heat transport (MHT) using

$$\text{MHT}(y, \theta) = \int_{C(y)} \rho_0 c_p \theta \, d\Psi_{y\theta}, \quad (14)$$

where ρ_0 is a reference density, c_p is the heat capacity of seawater, and $C(y)$ is a line of constant latitude in the latitude–temperature plane. Equation (14) represents the flux of heat in the meridional direction due to advection, at the latitude y. In the case of the thermohaline streamfunction, $\Psi_{\theta S}$ can be used to determine a heat function describing the flux of heat across isohalines and a salt function describing the flux of salt across isotherms.
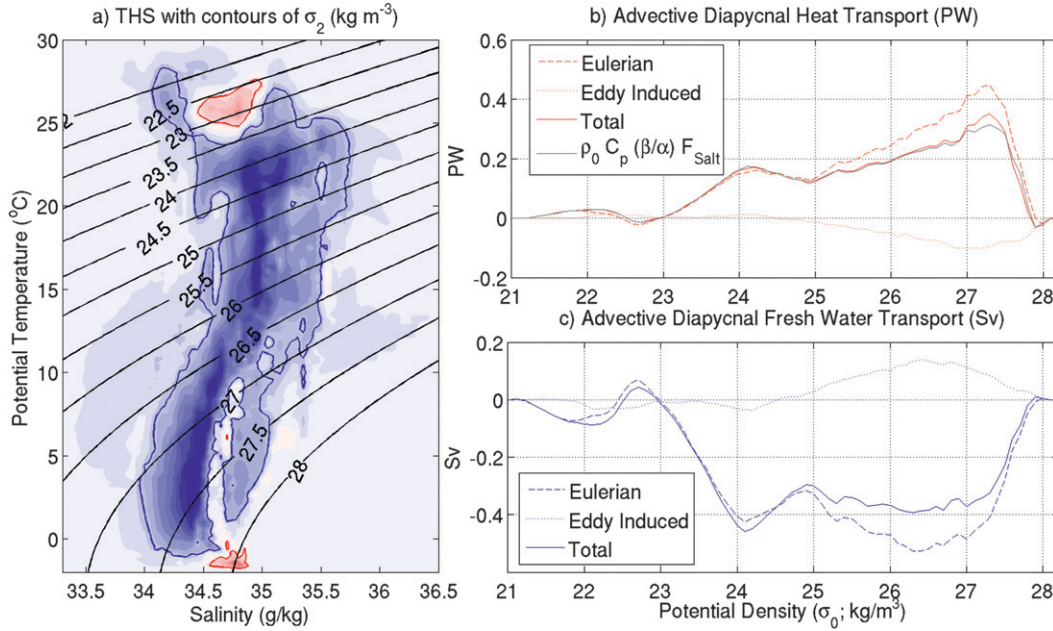
FIG. 8. (a) THS $\Psi_{\theta S}$ as in Fig. 6, but with contours of surface-referenced potential density σ_0 overlaid. (b) Diapycnal heat and (c) diapycnal freshwater flux from the ocean model computed directly from the THS. The freshwater flux is simply computed as $F_{\text{salt}}/35$ g kg^{-1}. The total (solid), Eulerian (dashed), and eddy-induced (dotted) components are shown. The gray line in (b) is the diapycnal heat flux as predicted by (20) given the diapycnal salt flux and the mean ratio β/α.

Because potential density is a function of temperature and salinity, a heat function and a salt function can also be defined, describing the flux of heat and salt across isopycnals. The total heat and salt transports across an isopycnal can then be determined from the thermohaline streamfunction using

$$F_{\text{Heat}}(\sigma) = \rho_0 c_p \int_{C(\sigma)} \theta \, d\Psi_{\theta S} \quad \text{and} \quad (15)$$

$$F_{\text{Salt}}(\sigma) = \int_{C(\sigma)} S \, d\Psi_{\theta S}, \quad (16)$$

where $C(\sigma)$ is a line of constant potential density in the temperature–salinity plane.

The salt transport can be converted into the more tangible "freshwater transport" F_{FW} in units of Sverdrups by $F_{\text{FW}} = -F_{\text{Salt}}/\overline{S}$. Here, we use $\overline{S} = 35$ g kg^{-1}. The resulting heat and freshwater transports across potential density surfaces (σ_0) from the ocean model simulation are shown in Fig. 8.

For most isopycnal ranges, the ocean transports heat toward denser waters and freshwater toward lighter waters. This is consistent with the large-scale balance between the ocean circulation and the ocean–atmosphere fluxes, with subtropical waters gaining heat but losing freshwater to the atmosphere, whereas dense polar waters lose heat but gain freshwater via air–sea exchange.

The framework of Walin (1982) relates surface transformations of a single property (e.g., density or temperature) to an advective flux across a constant property surface. With a given prescription of mixing, one can use observed surface fluxes and the mean hydrography to diagnose a streamfunction in, for example, property versus latitude coordinates (Greatbatch and Zhai 2007). However, such estimates are poorly constrained because of zonal averaging and the result depends purely on the mixing prescribed. Speer (1993) extends the framework of Walin (1982), relating surface heat and salt fluxes to a transport in temperature salinity coordinates. In addition, Zika et al. (2010b) provide a relationship between diapycnal and isopycnal mixing and transport across lines of constant temperature and salinity in the ocean interior. Our analysis suggests that, by combining the frameworks of Speer (1993) and Zika et al. (2010b), one could combine observed atmosphere–ocean heat and freshwater fluxes and theories about interior ocean mixing to provide a constrained estimate of the thermohaline streamfunction from observations.

The sign of the diapycnal heat and salt flux is evident geometrically from the thermohaline streamfunction itself. Clockwise cells advect heat and salt toward denser waters, and anticlockwise cells advect heat and salt toward lighter waters (Fig. 9). This symmetry between downward heat and freshwater fluxes is clear when considering the thermal and haline components of the
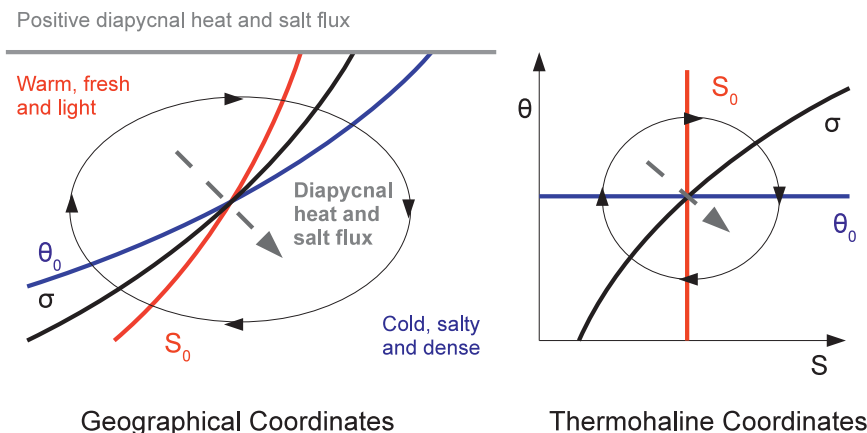
FIG. 9. Schematic describing the geometric relationship between the THS and diapycnal heat and salt fluxes. (left) If water is advected toward denser waters on the warmer and saltier parts of an isopycnal surface (σ), (right) this appears as a clockwise circulation in θ–S space. Because the same trajectory has different temperatures as it crosses the same isopycnal surface it represents a net positive diapycnal transport of heat and salt. The circulation shown in physical space [in (left)] can be both a horizontal (e.g., gyre in x–y space) circulation where this diapycnal transport is balanced by surface heating, cooling and evaporation minus precipitation and/or a vertical overturning (in z–y space) where the transport is balanced by interior mixing or nonlinear processes.

transport of density across an isopycnal. Given a thermal expansion coefficient α and haline contraction coefficient β, we have

$$F_\sigma(\sigma) = -\int_{C(\sigma)} \alpha\theta\, d\Psi_{\theta S} + \int_{C(\sigma)} \beta S\, d\Psi_{\theta S}, \quad (17)$$

$$= \int_{C(\sigma)} \sigma\, d\Psi_{\theta S}, \quad \text{and} \quad (18)$$

$$= \sigma \int_{C(\sigma)} d\Psi_{\theta S} = 0. \quad (19)$$

Hence, the thermal and haline contributions to the density flux are equal. In fact, if the ratio of α/β is approximately constant on a given σ surface (i.e., not necessarily for all θ and S), then the relationship between the diapycnal heat and salt flux is simply

$$\frac{F_{\text{Heat}}(\sigma)}{F_{\text{Salt}}(\sigma)} \approx \rho_0 c_p \frac{\beta}{\alpha}. \quad (20)$$

We approximate the diapycnal heat flux across σ_0 surfaces using (20), where we use the volume average ratio of α/β referenced to the surface [i.e., $\alpha(S, \theta, p = 0)/\beta(S, \theta, p = 0)$; Fig. 8]. We find that the relationship is near exact for $\sigma_0 < 26$ kg m^{-3}. The error reaches a maximum of 10% for denser waters. Such error may also be reduced with the use of a more globally consistent isopycnal coordinate such as neutral density.

The significance of this thermohaline symmetry is that, where there is a net advective heat flux across

isopycnals, freshwater must be advected in the opposite direction. Where the ocean advects heat toward denser water masses in steady state, it must advect freshwater toward lighter water masses. In an ongoing study, we investigate whether the symmetry between the ocean's diapycnal heat and salt transport has broader implications for the global climate system. It may be that the balance described above places constraints on the relationship between large-scale atmospheric moisture transport and ocean heat transport.

6. Thermohaline transit time

Given the thermohaline streamfunction and estimates of the mean gradients of temperature and salinity, we can gain a measure of the time taken for a water parcel to make a full circuit in θ–S space. We name this measure the thermohaline transit time $\mathcal{T}_{\theta S}$. As discussed in the next section, individual water parcels, even in the absence of dispersion, do not complete closed "loops" in θ–S space, as with any three-dimensional flow. However, the concept of transit time is insightful because it provides a measure of the minimum time for a water parcel to be advected in this coordinate system.

For a fluid parcel following a streamline in θ–S space, the time increment $dt|_\Psi$ for given θ and S increments $d\theta|_\Psi$ and $dS|_\Psi$ is

$$dt|_\Psi = \frac{Dt}{D\theta} d\theta|_\Psi + \frac{Dt}{DS} dS|_\Psi. \quad (21)$$

That is, the time taken for a fluid parcel to change temperature by an amount $d\theta|_\Psi$ and change salinity by $dS|_\Psi$ depends on both the rate of change of temperature following the fluid parcel $D\theta/Dt$ and the rate of change of salinity following the fluid parcel DS/Dt. If θ and S are steady, fluid parcels change temperature and salinity when they are advected down a temperature or salinity gradient such that

$$\frac{D\theta}{Dt} = \mathbf{u} \cdot \nabla\theta; \quad \frac{DS}{Dt} = \mathbf{u} \cdot \nabla S. \quad (22)$$

We now seek an approximation for the right-hand sides of (22) based on quantities averaged in thermohaline coordinates such as the thermohaline streamfunction. By computing $\Psi_{\theta S}$ from (10), we have naturally computed an integral of both components of the velocity needed in (22) because (10) can be written as

$$\Delta\Psi_{\theta,\Delta S} = \frac{1}{\Delta t}\int_t^{t+\Delta t}\int_S^{S+\Delta S}\frac{\mathbf{u}\cdot\nabla\theta}{|\nabla\theta|}\,dA|_\theta\,dt \quad \text{and} \quad (23)$$

$$\Delta\Psi_{S,\Delta\theta} = \frac{1}{\Delta t}\int_t^{t+\Delta t}\int_\theta^{\theta+\Delta\theta}\frac{\mathbf{u}\cdot\nabla S}{|\nabla S|}\,dA|_S\,dt. \quad (24)$$

Defining areas $\Delta A_{\theta,\Delta S}$ and $\Delta A_{S,\Delta\theta}$ as

$$\Delta A_{\theta,\Delta S} = \frac{1}{\Delta t}\int_t^{t+\Delta t}\int_S^{S+\Delta S}dA|_\theta\,dt \quad \text{and} \quad (25)$$

$$\Delta A_{S,\Delta\theta} = \frac{1}{\Delta t}\int_t^{t+\Delta t}\int_\theta^{\theta+\Delta\theta}dA|_S\,dt \quad (26)$$

and area averages $\langle\rangle_{\theta,\Delta S}$ and $\langle\rangle_{S,\Delta\theta}$ such that

$$\langle|\nabla\theta|\rangle_{\theta,\Delta S} = \frac{1}{\Delta t\Delta A_{\theta,\Delta S}}\int_t^{t+\Delta t}\int_S^{S+\Delta S}|\nabla\theta|\,dA|_\theta\,dt \quad \text{and} \quad (27)$$

$$\langle|\nabla S|\rangle_{S,\Delta\theta} = \frac{1}{\Delta t\Delta A_{S,\Delta\theta}}\int_t^{t+\Delta t}\int_\theta^{\theta+\Delta\theta}|\nabla S|\,dA|_S\,dt, \quad (28)$$

we may derive a quantity with units of velocity using the following approximation:

$$V_{S,\Delta\theta} = \frac{\Delta\Psi_{\theta,\Delta S}}{\Delta A_{\theta,\Delta S}} = \left\langle\frac{\mathbf{u}\cdot\nabla\theta}{|\nabla\theta|}\right\rangle_{\theta,\Delta S} \approx \frac{\langle\mathbf{u}\cdot\nabla\theta\rangle_{\theta,\Delta S}}{\langle|\nabla\theta|\rangle_{\theta,\Delta S}} \quad \text{and} \quad (29)$$

$$V_{\theta,\Delta S} = \frac{\Delta\Psi_{S,\Delta\theta}}{\Delta A_{S,\Delta\theta}} = \left\langle\frac{\mathbf{u}\cdot\nabla S}{|\nabla S|}\right\rangle_{S,\Delta\theta} \approx \frac{\langle\mathbf{u}\cdot\nabla S\rangle}{\langle|\nabla S|\rangle_{S,\Delta\theta}}. \quad (30)$$

The approximation above implies that the gradients of temperature and salinity and/or the velocity down those gradients should not vary greatly at constant temperature
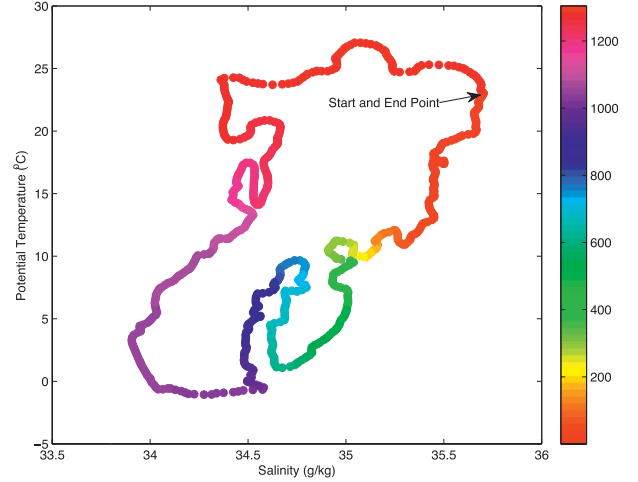
FIG. 10. The accumulated thermohaline transit of the -4-Sv streamline. The color of each dot represents the relative time taken along the streamline estimated using only the THS itself and the mean θ–S gradients.

and salinity. From the θ and S fields of the model, we can compute $\langle|\nabla\theta|\rangle_{\theta,\Delta S}$ and $\langle|\nabla S|\rangle_{S,\Delta\theta}$. Thus, from (22) we have

$$\frac{D\theta}{Dt} \approx V_{\theta,\Delta S}\langle|\nabla\theta|\rangle_{\theta,\Delta S};$$
$$\frac{DS}{Dt} \approx V_{S,\Delta\theta}\langle|\nabla S|\rangle_{S,\Delta\theta}. \quad (31)$$

Substituting into (21) then yields

$$dt|_\psi \approx \frac{1}{V_{\theta,\Delta S}\langle|\nabla\theta|\rangle_{\theta,\Delta S}}d\theta|_\Psi + \frac{1}{V_{S,\Delta\theta}\langle|\nabla S|\rangle_{S,\Delta\theta}}dS|_\Psi. \quad (32)$$

One can then estimate the accumulated time $\mathcal{T}_{\theta S}$ following a $\Psi_{\theta S}$ streamline by integrating (32) such that

$$\mathcal{T}_{\theta S} = \int_0^{\mathcal{T}}dt|_\Psi$$
$$\approx \int_{\theta(0)}^{\theta(\mathcal{T})}\frac{1}{V_{\theta,\Delta S}\langle|\nabla\theta|\rangle_{\theta,\Delta S}}d\theta|_\Psi$$
$$+ \int_{S(0)}^{S(\mathcal{T})}\frac{1}{V_{S,\Delta\theta}\langle|\nabla S|\rangle_{S,\Delta\theta}}dS|_\Psi. \quad (33)$$

Here, we calculate $\mathcal{T}_{\theta S}$ by following the longest -4-Sv streamline in θ–S space (Fig. 10) and beginning the circuit at the saltiest point ($S = 35.7$ g kg^{-1}, $\theta = 23°$C), although the total thermohaline transit time is independent of the start point following a given streamline. The full circuit takes 1350 yr using (33). The cumulative time taken along the contour shows how the fluid moves from the initial warm salty waters toward cooler high
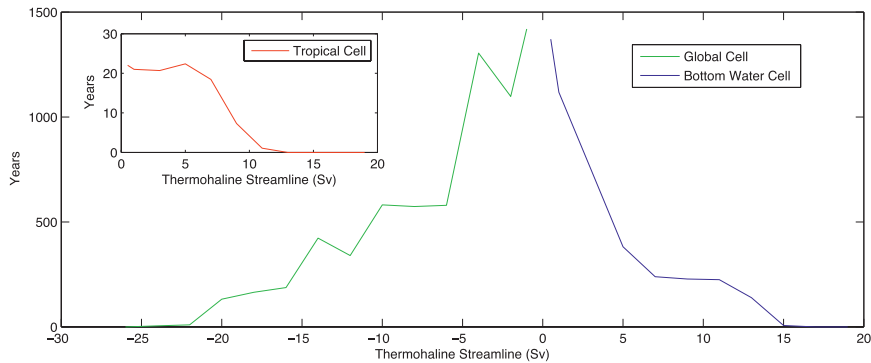
FIG. 11. The thermohaline transit time of the longest THS streamlines in θ–S space (i.e., the longest streamlines in Fig. 6 for each transport). Shown are transit times for the global cell (green), the bottom water cell (temperatures below 10°C, blue), and the tropical cell contours (longest positive streamlines with temperatures above 10°C, red). The Antarctic Bottom Water transit times may be underestimated because of interpolation onto a coarse θ–S grid.

saline waters at 10°C and 35.5 g kg^{-1} in a relatively short time scale of 100 yr or so. This short time scale is because of the strong, near-surface wind-driven circulation allowing rapid transitions between different water masses. There is then a gradual transition from the 10°C water through NADW to a local minimum in temperature of 2°C. The transit from this water mass (NADW) to the cold fresh waters around 0°C and 34.5 g kg^{-1}, a relatively short distance in θ–S space, takes the considerable majority of the remaining total transit. These dense water masses are found only in the deep ocean, where advection is weak and temperature and salinity gradients are small, meaning water-mass transitions occur gradually.

The total thermohaline transit times of THS contours are shown in Fig. 11. In each case, we take the longest streamline for a given transport value. The tropical cell, defined as the closed anticlockwise contours warmer than 10°C, has the shortest transit times on the order of 20 yr. For the global cell and its subcells, the transit times range from hundreds of years and asymptote to around 1500 yr for the −2-Sv contour. We do not discern between subcells in the warmer or colder portions of the global cell. The longest bottom water cell transit times are equivalent to the global cell on the order of 1500 yr. Increased resolution of the THS in θ–S space may change the bottom water transit times estimated here.

7. Basin-specific flow and water-mass pathways

Here, we address whether streamlines in thermohaline space correspond to pathways of individual water parcels or whether this circulation is simply the accumulation of many geographically independent cells. To answer this question, we start by investigating the nature of the THS in separate geographical regions where such a separation is possible.

The North Atlantic is generally saltier than the Indian and Pacific basins. However, the two share waters of like θ–S properties. Looking at the maximum temperatures and salinities along the sections that separate the Atlantic from the Indo-Pacific, we can determine θ–S ranges that are either wholly within the Atlantic or wholly within the Indo-Pacific and of course not in the Southern Ocean. That is, although like θ–S properties may exist in both basins, they are not geographically linked at any time. Any volume transport from Atlantic water to Indo-Pacific water must occur through some other intermediary θ–S range.

The θ–S ranges we choose for this strictly "non–Southern Ocean" water comprise all waters with either $S > 35$ g kg^{-1} or $\theta > 21.5$°C or waters where both $S < 34.8$ g kg^{-1} and $\theta > 16$°C (i.e., only those regions in θ–S space that have green or red contours in Fig. 12) . Any water in that range is either in the Atlantic or in the Indo-Pacific but not in the Southern Ocean. Hence, a streamfunction can be defined independently by integrating from $\theta = \infty$ back to the edge of this domain in θ–S space. The result and the geographical domain of the two water masses are shown in Fig. 12. The streamlines for the Indo-Pacific are shown in green and for the Atlantic are shown in red. Clearly, the wide, anvil shape of the global THS is the result of a combination of a fresher Indo-Pacific branch and a saltier Atlantic branch. The warmest saltiest waters only exist in the Atlantic, and the coldest freshest waters only exist in the Indo-Pacific. The Indo-Pacific takes freshwater from the deep or southern waters and returns them as saltier waters, whereas the Atlantic takes intermediate salinity waters and returns them as high salinity waters.

The same decomposition as is done for the warmest waters by ocean basin can be done for the coldest freshest waters by hemisphere. Cold freshwater exists in
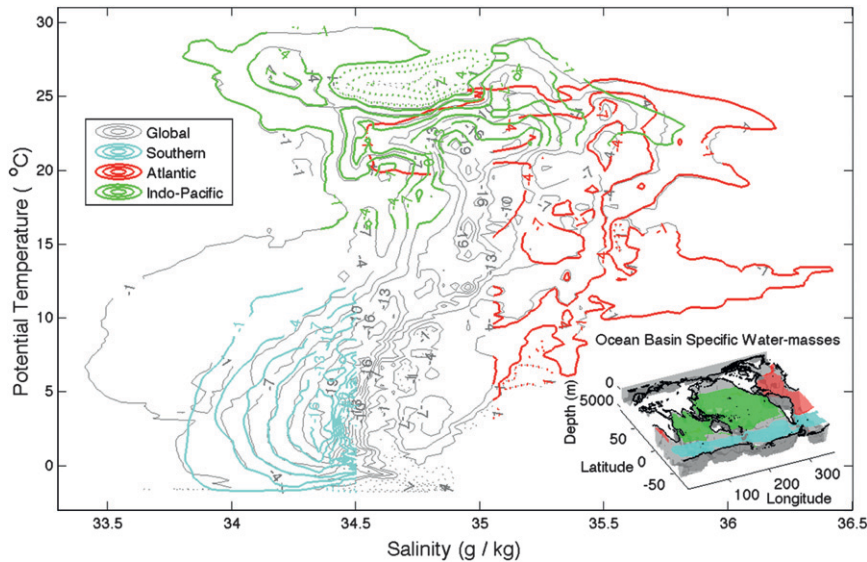
FIG. 12. The THS for various oceanic regions. Shown are THS for water masses found only in the Indian and Pacific basins (green; green volume in insert), water masses found only in the Atlantic (red), and finally water masses found only in the Southern Ocean (blue).

both the Southern Ocean and the Arctic–North Pacific. However, no cold freshwater exists around the equator. Hence, we can partition the two. Specifically, we compute a streamfunction only for waters with $\theta < 12°C$ and $S < 34.5$ g kg^{-1} for each hemisphere. The resulting Southern Ocean streamfunction is almost the same as that derived from the sum of both the Northern and Southern Hemispheres, demonstrating the dominant role of the Southern Ocean in the circulation in this $\theta–S$ range.

An interpretation of the global water-mass pathway thus emerges of water moving from the Atlantic to the Southern Ocean and into the Pacific. We now attempt to track this pathway more precisely by following a streamline from one basin to the next. We take the THS plotted in Fig. 12 and follow the $\theta–S$ values corresponding to the longest -4 Sv streamline. We start with the freshest point in the Atlantic on this contour. This contour is tracked until the edge of the Atlantic water mass is reached at $S = 35$ g kg^{-1}. At this point the Atlantic streamfunction matches the global one. Continuing along the global streamline to $S = 34.5$ g kg^{-1}, the global THS matches almost perfectly with the Southern Ocean and again to $\theta = 12°C$, where it matches with the Pacific. Although one could continue indefinitely, we stop where this streamline reaches $\theta = 21.5°C$ and $S > 34.5$ g kg^{-1}. By allowing streamlines to transit from one basin to the next, the circulation is no longer closed and no one cell exists in a unique sense.

To determine the possible geographical route of water parcels along this thermohaline pathway, we color water masses in the ocean according to their location in $\theta–S$ space. For each point along the contour, a color is chosen corresponding to the distance along the contour: distance being in $\theta–S$ space, not geographical space. The color is then used to label the actual points in the ocean that have that temperature and salinity. The resulting analysis is shown in Fig. 13. Following the pathway as it moves from the surface Atlantic to the North Atlantic, then down into the deep ocean, and eventually up into the Southern Ocean and out into the North Pacific reveals a pathway reminiscent of the schematic diagrams of the thermohaline circulation, which was first depicted by Gordon (1986). We have presented here a method for diagnosing pathways of the thermohaline circulation that is complimentary to more explicit Lagrangian diagnostic approaches (e.g., Blanke et al. 2001).

An important difference between the conveyor of Gordon (1986) and Broecker (1991) and that revealed by Fig. 13 is that the model diagnosed THS transits through the surface waters of the Southern Ocean with significant transformation of $\theta–S$ properties. This is despite the meridional overturning in density space showing North Atlantic Deep Water upwelling diapycnally at midlatitudes (Fig. 2). This suggests that waters are exchanged meridionally at constant density but enter and exit with different temperatures and salinities (i.e., different spiciness).

8. Summary and conclusions

The circulation of a global ocean model has been presented in temperature salinity coordinates for the
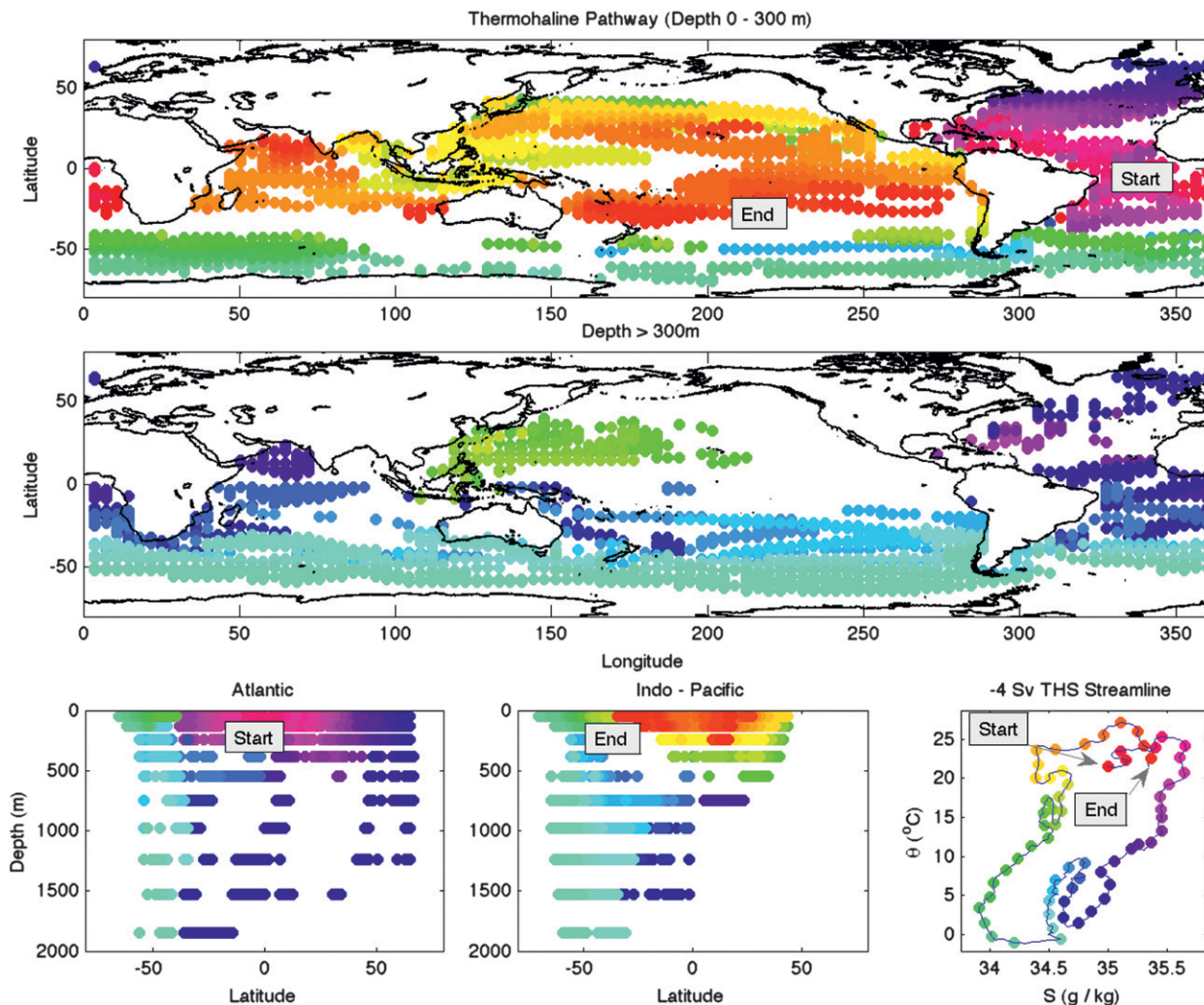
FIG. 13. (bottom right) A thermohaline pathway projected into physical space. The −4-Sv THS contour is followed from the Atlantic water masses (red in Fig. 12) to the Southern Ocean (blue in Fig. 12) and then finally to the Indo-Pacific water masses. At points equally spaced in θ–S space along the contour, a color is chosen to represent water masses with those water-mass properties. All grid boxes in the corresponding region with potential temperatures and salinities within 0.1°C and 0.05 g kg^{-1}, respectively, of that point in θ–S space are then assigned the color of that point. (top) All grid boxes above 300 m. (middle) All grid boxes below 300 m. (bottom left) Only Atlantic grid boxes. (bottom middle) Indo-Pacific grid boxes.

first time. The resulting THS distills the ocean circulation into three distinct cells: a tropical warm cell, a "global cell," and an Antarctic Bottom Water cell. Many of the streamlines (around 4–5 Sv) of the global cell link the cold and salty waters of the North Atlantic to the warm fresh waters of the Indo-Pacific, providing a quantification of the "global conveyor" or thermohaline circulation. Here, we have analyzed the ocean component of an equilibrated global climate model. The presence of a global cell in thermohaline coordinates is also confirmed in an upcoming study by Döös et al. (2012), who compute the thermohaline streamfunction of an eddy permitting ocean model.

A number of novel advantages of computing a thermohaline streamfunction are also revealed. First, the THS can be used to diagnose the role of resolved and parameterized transient fluxes in water-mass transformation zones. Parameterized transient eddy fluxes are found to be leading order across the majority of water-mass classes. Averaging in thermohaline space provides a framework in which the role of diabatic processes and parameterized fluxes are highlighted.

Second, once the circulation is averaged in thermohaline coordinates, diapycnal heat and salt transports are easily quantified. Clockwise cells in thermohaline space flux heat and salt toward denser waters and anticlockwise

cells flux heat and salt toward lighter waters. We show that the ratio of the diapycnal flux of potential temperature to the diapycnal flux of salt may be approximated by β/α (the ratio of the haline contraction to thermal expansion coefficients). This relationship we find to be accurate to within 10% error. In our model, heat and salt are transported from light waters to dense waters by the clockwise global cell. Heat and salt are transported from light waters associated with subtropical latitudes to denser waters associated with polar regions. This poleward salt transport is in symmetry with the atmosphere's poleward transport of freshwater at subtropical to subpolar latitudes.

An ongoing study is investigating whether the symmetry between ocean diapycnal heat and salt fluxes places constraints on the meridional balances of ocean freshwater transport and atmospheric moisture transport. Pauluis et al. (2008) showed that the strength of the atmospheric circulation is different in dry-isentropic (potential temperature) and moist-isentropic (moisture plus potential temperature) coordinates because of a process dubbed the moist recirculation (Laliberté et al. 2012). An equivalent analysis to that presented here, analyzing the atmospheric circulation in "hydrothermal" (moisture–potential temperature) coordinates, may be illuminating.

Third, a measure of the transit time of the global conveyor, the thermohaline transit time, is readily quantified from the THS. The thermohaline transit time in our model is 1350 yr for typical streamlines associated with the global-scale conveyor. Such a simple diagnostic may prove useful in comparing the ventilation time of various models, especially in cases where the incorporation of more involved tracer diagnostics is prohibitive.

Finally, separating the THS by region, the Southern Ocean is found to dominate the coolest and freshest water masses. The THS trajectory from cool fresh waters to cool salty waters is the sum of both a fresher tropical–subtropical branch in the Indian and Pacific Oceans and a saltier tropical to subpolar branch in the Atlantic Ocean. The sum of these three branches reveals a globally interconnected circulation.

A major difference between the global conveyor of this model and the schematic view of Gordon (1986) and Broecker (1991) is that most of the diagnosed THS (-5 to -15 Sv; narrow core of the THS in Fig. 6) occurs at the surface rather than in deep waters. In addition, almost all streamlines (0 to -15 Sv) transit through the Southern Ocean. This is despite the majority of diapycnal upwelling in the model occurring in the abyssal ocean (Fig. 2). This implies that even a density space overturning, driven by interior diapycnal mixing, may still transit through the Southern Ocean in order for the global balances of heat and salt to be maintained.

REFERENCES

Blanke, B., S. Speich, G. Madec, and K. Döös, 2001: A global diagnostic of interocean mass transfers. *J. Phys. Oceanogr.,* **31,** 1623–1632.

——, M. Arhan, and S. Speich, 2006: Salinity changes along the upper limb of the Atlantic thermohaline circulation. *Geophys. Res. Lett.,* **33,** L06609, doi:10.1029/2005GL024938.

Boccaletti, G. R., R. Ferrari, A. Adcroft, D. Ferreira, and J. Marshal, 2005: The vertical structure of ocean heat transport. *Geophys. Res. Lett.,* **32,** L10603, doi:10.1029/2005GL022474.

Broecker, W. S., 1991: The great ocean conveyor. *Oceanography,* **4,** 79–89.

Cuny, J., P. B. Rhines, P. P. Niiler, and S. Bacon, 2002: Labrador Sea boundary currents and the fate of the Irminger Sea Water. *J. Phys. Oceanogr.,* **32,** 627–647.

Davis, R. E., R. de Szoeke, D. Halpern, and P. Niiler, 1981: Variability in the upper ocean during MILE. Part I: The heat and momentum balances. *Deep-Sea Res.,* **28,** 1427–1452.

Deacon, G. E. R., 1937: *The Hydrology of the Southern Ocean.* Vol. 15, *Discovery Reports,* Cambridge University Press, 124 pp.

Döös, K., and D. Webb, 1994: The Deacon cell and other meridional cells of the Southern Ocean. *J. Phys. Oceanogr.,* **24,** 429–442.

——, J. Nilsson, J. Nycander, and L. Brodeau, 2012: The World Ocean thermohaline circulation. *J. Phys. Oceanogr.,* in press.

Ferrari, R., and D. Ferreira, 2011: What processes drive the ocean heat transport? *Ocean Modell.,* **38,** 171–186.

Gent, P. R., and J. C. McWilliams, 1990: Isopycnal mixing in ocean circulation models. *J. Phys. Oceanogr.,* **20,** 150–155.

Gordon, A. L., 1986: Interocean exchange of thermocline water. *J. Geophys. Res.,* **91,** 5037–5046.

——, 1991: The role of thermohaline circulation in global climate change. Lamont-Doherty Geological Observatory 1990 and 1991 Report, Lamont-Doherty Earth Observatory Tech. Rep., 44–51.

Greatbatch, R. J., and X. Zhai, 2007: The generalized heat function. *Geophys. Res. Lett.,* **34,** L21601, doi:10.1029/2007GL031427.

Griffies, S., 2007: *Fundamentals of Ocean Climate Models.* Princeton University Press, 230 pp.

Kuhlbrodt, T., A. Griesel, M. Montoya, A. Levermann, M. Hofmann, and S. Rahmstorf, 2007: On the driving processes of the Atlantic meridional overturning circulation. *Rev. Geophys.,* **45,** RG2001, doi:10.1029/2004RG000166.

Laliberté, F., T. Shaw, and O. Pauluis, 2012: Moist recirculation and water vapor transport on dry isentropes. *J. Atmos. Sci.,* **69,** 875–890.

Manabe, S., K. Bryan, and M. J. Spelman, 1990: Transient response of a global ocean-atmosphere model to a doubling of atmospheric carbon dioxide. *J. Phys. Oceanogr.,* **20,** 722–749.

Marsh, R., S. A. Josey, A. J. G. de Nurser, B. A. Cuevas, and A. C. Coward, 2005: Water mass transformation in the north atlantic over 1985–2002 simulated in an eddy-permitting model. *Ocean Sci.,* **1,** 127–144.

McDougall, T. J., 2003: Potential enthalpy: A conservative oceanic variable for evaluating heat content and heat fluxes. *J. Phys. Oceanogr.,* **33,** 945–963.

——, D. R. Jackett, and F. J. Millero, 2009: An algorithm for estimating absolute salinity in the global ocean. *Ocean Sci. Discuss.,* **6,** 215–242.

Munk, W. H., and K. Wunsch, 1998: Abyssal recipes II: Energetics of tidal and wind mixing. *Deep-Sea Res.,* **45,** 1977–2010.

Nurser, A. J. G., and R. Marsh, 1998: Water mass transformation theory and the meridional overturning streamfunction. *International WOCE Newsletter,* No. 31, WOCE International Project Office, Southampton, United Kingdom, 36–38.

——, and M.-M. Lee, 2004: Isopycnal averaging at constant height. Part I: The formulation and a case study. *J. Phys. Oceanogr.,* **34,** 2721–2739.

Nycander, J., J. Nilsson, K. Döös, and G. Bromström, 2007: Thermodynamic analysis of ocean circulation. *J. Phys. Oceanogr.,* **37,** 2038–2052.

Pacanowski, R., 1995: MOM2 documentation users guide and reference manual. GFDL Ocean Group Tech. Rep., 232 pp.

Pauluis, O., A. Czaja, and R. Korty, 2008: The global atmospheric circulation on moist isentropes. *Science,* **321,** 1075.

Richardson, P. L., 2008: On the history of meridional overturning schematic diagrams. *Prog. Oceanogr.,* **76,** 466–486.

Schmitz, W. J., Jr., 1996: On the world ocean circulation. Volume I: Some global features/North Atlantic circulation. Woods Hole Oceanographic Institute Tech. Rep. WHOI–96–03, 140 pp.

Sijp, W. P., M. Bates, and M. H. England, 2006: Can isopycnal mixing control the stability of the thermohaline circulation in ocean climate models? *J. Climate,* **19,** 5637–5651.

Speer, K. G., 1993: Conversion among North Atlantic surface water types. *Tellus,* **45,** 72–79.

Stommel, H., and A. B. Arons, 1960: On the abyssal circulation of the worlds ocean—II. An idealized model of circulation pattern and amplitude in oceanic basins. *Deep-Sea Res.,* **6,** 140–154.

Walin, G., 1982: On the relation between sea-surface heat flow and thermal circulation in the ocean. *Tellus,* **34,** 187–195.

Wüst, G., 1935: Die stratosphäre des Atlantischen Ozeans. *Wissenschaftliche Ergebnisse der Deutschen Atlantischen Expedition auf dem Forschungs und Vermessungsschiff, Meteor 1925–1927,* Gruyter & Co., 109–288.

Zika, J. D., and T. J. McDougall, 2008: Vertical and lateral mixing processes deduced from the Mediterranean Water signature in the North Atlantic. *J. Phys. Oceanogr.,* **38,** 164–176.

——, B. M. Sloyan, and T. J. McDougall, 2009: Diagnosing the Southern Ocean Overturning from tracer fields. *J. Phys. Oceanogr.,* **39,** 2926–2940.

——, T. J. McDougall, and B. M. Sloyan, 2010a: A tracer-contour inverse method for estimating ocean circulation and mixing. *J. Phys. Oceanogr.,* **40,** 26–47.

——, ——, and ——, 2010b: Weak mixing in the eastern North Atlantic: An application of the tracer-contour inverse method. *J. Phys. Oceanogr.,* **40,** 1881–1893.